Queensland University of Technology
Brisbane Australia

This is the author's version of a work that was submitted/accepted for publication in the following source:

Kristof, Janos, Szilagyi, Tamas, Horvath, Erzsebet, De Battisti, Achille, Frost, Ray L., & Redey, Akos (2004) Investigation of IrO2/Ta2O5 thin film evolution. *Thermochimica Acta*, *413*(1-2), pp. 93-99.

This file was downloaded from: http://eprints.qut.edu.au/21748/

© Copyright 2004 Elsevier

Notice: *Changes introduced as a result of publishing processes such as copy-editing and formatting may not be reflected in this document. For a definitive version of this work, please refer to the published source:*

http://dx.doi.org/10.1016/j.tca.2003.10.019

Investigation of IrO_2/Ta_2O_5 Thin Film Evolution

János Kristóf,[*a] Tamás Szilágyi,[a] Erzsébet Horváth,[b] Achille De Battisti,[c] Ray L. Frost,[d] and Ákos Rédey[b]

[a]*University of Veszprém, Department of Analytical Chemistry, H-8201 Veszprém, P.O.Box 158, Hungary,*

[b]*University of Veszprém, Department of Environmental Engineering and Chemical Technology, H-8201 Veszprém, P.O.Box 158, Hungary,*

[c]*University of Ferrara, via L. Borsari 46, I-44100 Ferrara, Italy*

[d]*Queensland University of Technology, School of Physical and Chemical Sciences, 2 George Street, GPO Box 2434, Q-4001, Brisbane, Australia,*

Keywords: oxide anodes, thin films, sol-gel process, IrO_2, Ta_2O_5, thermogravimetry-mass spectrometry (TG-MS), infrared emission spectroscopy (IRES)

[*]To whom correspondence should be addressed. Phone/Fax: +36 88 421 869, Email: kristof@almos.vein.hu

Abstract

The thermal evolution process of IrO_2 - Ta_2O_5/Ti coatings with varying noble metal content has been investigated under *in situ* conditions by thermogravimetry combined with mass spectrometry. The gel-like films prepared from alcoholic solutions of the precursor salts ($IrCl_3 \cdot 3H_2O$ and $TaCl_5$) onto titanium metal support were heated in an atmosphere containing 20% O_2 and 80% Ar up to 600 °C. The liberation of the chlorinated species followed by the mass spectrometric ion intensity curves showed that the two oxide phases do not develop independently.

The cracking of retained solvent, the combustion of organic surface species formed (and elemental carbon trapped in the film) was also followed by the MS curves. The formation of carbonyl- and carboxylate-type surface species connected to the noble metal were identified by Fourier transform infrared emission spectroscopy. These secondary processes -catalyzed by the noble metal- play an important role in the development of surface morphology of the films when used as anode materials in oxygen evolution reactions.

Introduction

Thermally prepared IrO_2 –based coatings deposited on titanium metal supports are the most promising anodes in electrometallurgy where cheaper, but environmentally undesired materials like e.g. lead alloys, have to be dismissed. [1,2] More generally, other industrial processes where oxygen evolution is one of the electrochemical reactions occurring at the anode (e.g. electrochemical oxidation or incineration of organics in aquatic media), may represent important potential fields of application for the above electrode materials. [3,4] Tantalum pentoxide is often suggested as the optimal stabilizing component of IrO_2-based film anodes and, independently from this application, Ta_2O_5 films have a growing potential in microelectronics as capacitors in high density dynamic random access memories (DRAMs), [5-7] as light waveguides, [8-10] or as antireflection coatings. [11-14]

Among the many IrO_2-based film electrodes, an important advantage offered by mixed oxide coatings consisting of IrO_2 and Ta_2O_5 is the remarkable catalytic activity for the oxygen evolution reaction, which allows to carry out the process of interest with lower energy consumption. [15-23] The decisive feature is, however, the service life of these electrodes, which are so far satisfactory for many practical applications, in spite of the fact that the performance can be still improved by proper optimization of the electrode film preparation.

The conventional thermal deposition method of film preparation involves the use of $H_2IrCl_6 \cdot 6H_2O$ and $TaCl_5$ precursors dissolved in hydrochloric acid and alcohol, respectively. [24] It was reported that oxide anodes prepared from organic solvent systems display better performance. [25,26] It was also shown that IrO_2 - Ta_2O_5 coatings prepared at low temperature display a low stability due to incomplete thermal decomposition resulting in the dissolution of the coating during electrolysis. [27,28] At higher temperatures (>500 °C), however, partial oxidation of the base metal leads to low adhesion of the film to the support. Therefore, an *in situ* study of the thermolysis processes is indispensable in order to improve

the design of thermally prepared electrode coatings. In the present work the thermal evolution process of the IrO_2 - Ta_2O_5 system prepared by the sol-gel method is studied in detail using thermogravimetry - mass spectrometry and infrared emission spectroscopy.

Experimental section

Thin film preparation. The precursor salts -$IrCl_3 \cdot 3H_2O$ (Fluka, Buchs, Switzerland) and $TaCl_5$ (Sigma-Aldrich, Budapest, Hungary) were dissolved in 2-propanol and a 0.05M stock solution was prepared for each component. Mixtures of varying compositions of the precursor salts (using the 0.05 M stock solutions) were made from 0% Ir to 100% Ir (at mole fraction) with 10% Ir steps. The precursor salt mixtures were prepared onto titanium metal supports (size 4mm x 4mm, thickness 0.1mm) etched in boiling oxalic acid (10%) for 15 minutes, washed with distilled water, rinsed with acetone and dried at room temperature. The coatings were prepared by applying the precursor salt solution (after a 10-fold dilution with 2-propanol) drop by drop onto the support and removing the solvent by hot air (60°C). This procedure was continued until a measurable quantity of the gel-like film (1-5 mg) corresponding to a relatively thick (400-800 nm) layer was deposited.

Thermoanalytical investigations. Thermoanalytical investigations and the heat treatment of the gel-like coatings were carried out in a Netzsch (Selb, Germany) TG 209 type thermobalance in a flowing gas atmosphere containing 19.8% oxygen and 80.2% argon (Messer Griesheim, Hungary). The purity of the gas mixture was 99.995%, and the heating rate was 10 °C/min. In order to follow simultaneously the evolution of the gaseous decomposition products over the temperature range from ambient to 600 °C, the thermobalance was connected to a Balzers MSC 200 Thermo-Cube type mass spectrometer (Balzers AG, Lichtenstein). The transfer line to introduce gaseous decomposition products

into the mass spectrometer was a deactivated fused silica capillary (Infochroma AG, Zug, Switzerland; 0.23 mm o.d.) temperature controlled to 150 °C to avoid condensation of high-boiling organic matter.

Fourier Transform Infrared Emission Spectroscopic (IRES) analyses. FT-IR emission spectroscopic measurements were carried out in a Digilab FTS-60A spectrometer, which was modified by replacing the IR source with an emission cell. The infrared emission cell consists of a modified atomic absorption graphite rod furnace, which is driven by a thyristor-controlled AC power source capable of delivering up to 150 amps at 12 volts. A platinum disk acts as a hot plate to heat the titanium sheets with the coatings on top. An insulated 125 μm type R thermocouple was embedded inside the platinum plate in such a way that the junction was < 0.2 mm below the platinum surface. The operating temperature was controlled to ± 2 °C using an Eurotherm Model 808 proportional temperature controller, connected to the thermocouple. The emission spectra were collected at 50 °C intervals in the 150 - 500°C range. The spectra were acquired by coaddition of 64 scans at a resolution of 4 cm^{-1}.

Results and Discussion

The thermogravimetric (mass loss, TG) and mass spectrometric ion intensity curves of 4.100 mg $TaCl_5$ gel on titanium metal support are given in Figure 1. The mass spectrometric ion intensity curves of the m/z = 35 ($^{35}Cl^+$), m/z = 41 ($C_3H_5^+/C_2HO^+$), and m/z = 44 (CO_2^+) fragments are of utmost importance to reveal the complicated mechanism of decomposition. By comparing the curves, the following conclusions can be drawn. Below 100 °C residual solvent (2-propanol), crystallization water, and hydrogen chloride (as a result of an intramolecular hydrolysis) are released. [29] In the mass loss stage between 120 and 200 °C alcoholic fragments ($C_3H_5^+/C_2HO^+$) are liberated indicating the presence of residual solvent in

the film. A detailed analysis of the residual organic matter with diffuse reflectance Fourier transform infrared spectroscopic (DRIFT) technique has already been made. [29] Chlorinated species also evolve in this range and their liberation is continued up to 500 °C in a rather uniform rate resulting in an almost linear mass loss stage. It is interesting to note that a small amount of CO_2 is also formed between 100 and 200 °C (at 161 °C with maximum rate), indicating the occurrence of combustion processes as well. The low temperature CO_2 formation is due to the burning (oxidative cracking) of residual alcohol. Since no organic cracking products are detected over 300 °C, it can be concluded that -in accordance with DRIFT data- no organic surface species are present in the temperature range of film solidification. Between 500 and 600 °C a dramatic change can be observed in the film evolution pattern. Chlorine is liberated in a fast reaction accompanied with the formation of CO_2 with maximum rate at 544 °C. The appearance of CO_2 in the gas phase is due to the combustion of elemental carbon formed and trapped in the film at lower temperature (between 120 and 200 °C).

The thermal evolution pattern of 1.628 mg $IrCl_3$ gel under identical experimental conditions is shown in Figure 2. Up to 150 °C residual alcohol and crystallization water is lost accompanied with a small amount of chloride formation (via intramolecular hydrolysis). Chlorine evolution takes place in two main stages at 319 and 561 °C. CO_2 appears at about 250 °C and is present until 450 °C as an evolved gas. The fact that the maximum rate of CO_2 liberation is observed at 400 °C (with an offset of some 80 °C with that of chlorine formation) indicates a combustion process independent of $IrCl_3$ oxidation.

In order to completely follow the process of thin film evolution, the changes in composition of the solid film should be followed as a function of the temperature, as well. Although infrared spectroscopy is a common tool to identify film composition, none of the traditional transmittance or reflectance methods can be used for the study of black, porous

films on metal supports. In infrared emission spectroscopy the infrared source is the heated sample itself. In principle, the emitted radiation (from thermally excited vibrational levels) can give exactly the same spectra as in absorption spectroscopy, but the signal to noise ratio (which is inherently low due to the low sample temperature) should be improved by the accumulation of spectra. Figure 3 shows the IRES spectrum of the $IrCl_3 \cdot 3H_2O$ gel heated at 180 °C. In accordance with earlier studies, Ir-carbonyls, carboxylates and IrO_x bands can be observed in the spectrum. [30] The bands of the organic surface species disappear by 400 °C, in harmony with the MS data. It can be concluded that -at variance with the Ta-system- complexation reactions take place in the presence of the noble metal.

The thermal evolution pattern of the 70% Ir-30% Ta system (Figure 4) shows close similarity to that of the 100 Ir system. The evolution of alcoholic fragments and CO_2 in the low temperature range occurs at 94 °C, a temperature lower by 22 °C than in the former case. The temperature of CO_2 evolution (352 °C) is also reduced by some 47 °C, while the first chlorine evolution stage is observed at 295 °C (reduced by 24 °C) and the second at 455 °C (reduced by 106 °C). It is interesting to observe that the film evolution process is finished (reaches its completeness) by 500 °C -a temperature lower by some 90 °C- indicating that the formation of the two oxide phases are not independent from each other.

The thermoanalytical curves of the 50%Ir-50%Ta system (Figure 5) differ significantly from those discussed above. The first chlorine evolution peak at 310 °C shows the close overlap of at least three independent processes, while the second one at approx. 475 °C is significantly reduced in intensity. While both chlorine peak temperatures increased by some 15-20 °C, the CO_2 peak temperature increased by 26 °C. It is more interesting, however, that the temperature range of CO_2 evolution reduced by half (from some 150 °C to approx. 75 °C). This drastic change indicates that the combustion of the organic surface species is catalyzed by the noble metal.

The thermal decomposition curves of the 30%Ir-70%Ta system (Figure 6) shows a much simpler pattern. Chlorine evolution can be observed in the 250 - 410 °C range in two overlapping processes -a slower and a faster one- accompanied with mass losses of similar amounts. The CO_2 evolution peak is rather sharp and of a symmetrical course, indicating combustion processes in the 370 - 420 °C range. It is also interesting to observe that the formation (solidification) of the mixed oxide film is finished by approx. 410 °C.

A comparison of the film evolution patterns reveal that the two oxide phases do not develop independently. This is due to the fact that tantalum pentoxide easily reacts with many other oxides to form mixed metal oxide phases of complex structure. [31] Although secondary ion mass spectrometric investigations confirmed the presence of iridium- and tantalum-containing mixed oxide clusters sputtered out of the film upon ion bombardment (e.g. $IrTaO^+$, $IrTaO_2^+$, $IrTa^+$), their intensity was very low (around the noise level), only. [32]

The temperature difference between the maxima of the two chlorine evolution peaks shows a minimum in the 30 to 50 % Ir range (Figure 7). Again, a monotonous change could be expected if the two oxide phases developed independently.

The peak temperature of CO_2 evolution shows a drastic decrease after the addition of 10% Ir to the $TaCl_5$ precursor (Figure 8). No significant change can be observed in the combustion temperature of organic surface species (and elemental carbon) at higher noble metal contents. It means that the combustion of organics is catalyzed by the noble metal and this process is practically independent of the evolution of the oxide phases.

The maximum temperature at which the removal (oxidative cracking) of residual solvent takes place is decreasing with the increase of the noble metal content, as well (Figure 9). Again, the catalytic effect of the noble metal on this degradation process can be witnessed. The simultaneous formation of CO_2 is an additional evidence of the fact that not only cracking but also a low temperature combustion of retained organics occurs.

Conclusion

Thermogravimetry - mass spectrometry combined with infrared emission spectroscopy can advantageously be used to follow the complicated process of film evolution. In addition to the development of the main (oxide) phases, side reactions that are of importance in the development of surface morphology (surface area, surface roughness, porosity) can be identified as well. These results are of importance when the experimental parameters necessary to obtain optimal electrochemical and surface properties are selected. In order to reveal the possible interactions between the two precursors, *in situ* investigations with e.g. small angle X-ray scattering and XPS are planned.

Acknowledgement

This research was supported by the Hungarian Scientific Research Fund under Grant OTKA T034355. The infrastructural support of the Queensland University of Technology in the frame of the Inorganic Materials Research Program is gratefully acknowledged.

References

(1) Trasatti, S. *Electrochim. Acta* **1999,** *45,* 2377.

(2) Trasatti, S. *Transition metal oxides: versatile materials for electrocatalysis,* in: Lipkowski, J.; Ross, P. (Eds.) *Electrochem. Novel Mater.,* VCH: New York, pp. 207-295, 1994.

(3) Jedral, W.; Merica, S.; Bunce, G. N. *Electrochem. Commun.* **1999,** *1,* 108.

(4) Foti, G.; Gandini, D.; Comninellis, Ch. *Curr. Topics in Electrochem.* **1997,** *5,* 71.

(5) Murawala, P. A.; Sawai, M.; Tatsuta, T.; Tsuji, O.; Fujita, S. *Jpn. J. Appl. Phys.* **1993,** *32,* 368.

(6) Shinriki, H.; Kisu, T.; Kimura, S.; Nishioka, Y.; Kawamoto, Y.; Mukai, K. *IEEE Trans. Electron Dev.* **1990,** *37,* 1939.

(7) Sankur, H. O.; Gunning, W. *Appl. Optics* **1989,** *28,* 2806.

(8) Tu, Y. K.; Lin, C. C.; Wang, W. S.; Huang, S. L. In *Optoelectronic Materials Devices Packaging and Interconnects;* Batchman, E.; Carson, R. F.; Galawa, R.L. (Eds.); SPIE Proc., SPIE: Bellingham, WA, Vol. 836, p. 40, 1987.

(9) Takahashi, H.; Suzuki, S.; Nishi, I. *J. Lightware Technol.* **1994,** *12,* 989.

(10) Chu, A. K.; Lin, H. C.; Cheng, W. H. *J. Electron. Mater.* **1997,** *26,* 889.

(11) Traylor-Kruschwitz, J. D.; Pawlewicz, W. T. *Appl. Opt.,* **1997,** *36,* 2157.

(12) Revesz, A. G.; Allison, J. F.; Reynolds, J. H. *Comsat Tech. Rev.* **1976,** *6,* 57.

(13) Hermann, W. C. Jr, *Vac. Sci. Technol.* **1981,** *18,* 1303.

(14) Motohiro, T.; Taga, Y. *Appl. Opt.* **1989,** *28,* 2466.

(15) De Nora, O.; Bianchi, G.; Nidola, A.; Trisoglio, G. US Patent, 3,878,083, 1975.

(16) Ferron, C. J.; Duby, P. F. in *EPD Congr. Proc. Symp. TMS Annu. Meet.* Hager, J. P. (Ed.), pp. 137-153, 1992.

(17) Hardee, K. L.; Ernes, L. M.; Carlson, R. C.; Thomas, D. E. US Patent, 5,167,788, 1992.

(18) Mraz, R.; Krysa, J. *J. Appl. Electrochem.* **1994,** *24,* 1262.

(19) Krysa, J.; Mraz, R. *Electrochim. Acta* **1995,** *40,* 1997.

(20) Krysa, J.; Kule, L.; Mraz, R.; Rousar, I. *J. Appl. Electrochem.* **1996,** *26,* 999.

(21) Krysa, J.; Maixner, J.; Mraz, R.; Rousar, I. *J. Appl. Electrochem.* **1998,** *28,* 369.

(22) Chen, X.; Chen, G.; Yue, P. L. *J. Phys. Chem. B* **2001,** *105,* 4623.

(23) Quattara, L.; Diaco, T.; Duo, I.; Panizza, M.; Foti, G.; Comninellis, Ch. *J. Electrochem. Soc.* **2003,** *150,* D41.

(24) Hine, F.; Yasuda, M.; Noda, T.; Yoshida, T.; Okuda, J. *J. Electrochem. Soc.* **1979,** *126,* 1439.

(25) Angelinetta, C.; Trasatti, S.; Atanasoska, L. D.; Minevski, Z. S.; Atanasoski R. T. *Mat. Chem. Phys.* **1989,** *22,* 231.

(26) Spindo, G.; Ardizzone, S.; Trasatti, S. *J. Electroanal. Chem.* **1997,** *423,* 49.

(27) Hu, J. M.; Meng, H. M.; Zhang, J. Q.; Cao, C. N. *Corr. Sci.* **2002,** *44,* 1655.

(28) Hu, J. M.; Wu, J.X.; Meng, H. M.; Sun, D. B.; Zhu, Y. R.; Yang, D. J. *Trans. Nonferrous Met. Soc. China (English Letters),* **2002,** *10,* 511.

(29) Kristof, J.; De Battisti, A.; Keresztury, G.; Horvath, E.; Szilagyi, T. *Langmuir,* **2001,** *17,* 1637.

(30) Mink, J.; Kristof, J.; De Battisti, A.; Daolio, S.; Németh, Cs. *Surf. Sci.* **1995,** *335,* 252.

(31) Ushikubo, T. *Catal. Today,* **2000,** *57,* 331.

(32) Daolio, S.; De Battisti, A.; Fabrizio, M.; Nanni, L.; Piccirillo, C. *Rapid Comm. Mass Spectrom.* **1998,** *12,* 1574.

Legends

Figure 1. TG (mass loss) and mass spectrometric ion intensity curves of $TaCl_5$ gel on titanium support.

Figure 2. TG (mass loss) and mass spectrometric ion intensity curves of $IrCl_3$ gel on titanium support.

Figure 3. FT-IR emission spectrum of an $IrCl_3$ gel heated at 180 °C on a titanium support.

Figure 4. TG (mass loss) and mass spectrometric ion intensity curves of the 70% Ir - 30% Ta system (sample mass: 1.591 mg).

Figure 5. TG (mass loss) and mass spectrometric ion intensity curves of the 50% Ir - 50% Ta system (sample mass: 2.560 mg).

Figure 6. TG (mass loss) and mass spectrometric ion intensity curves of the 30% Ir - 70% Ta system (sample mass: 1.990 mg).

Figure 7. The difference in chlorine evolution peak temperatures as a function of the Ir content.

Figure 8. The dependence of CO_2 evolution peak temperature on the Ir content.

Figure 9. The dependence of solvent evolution peak temperature on the Ir content.

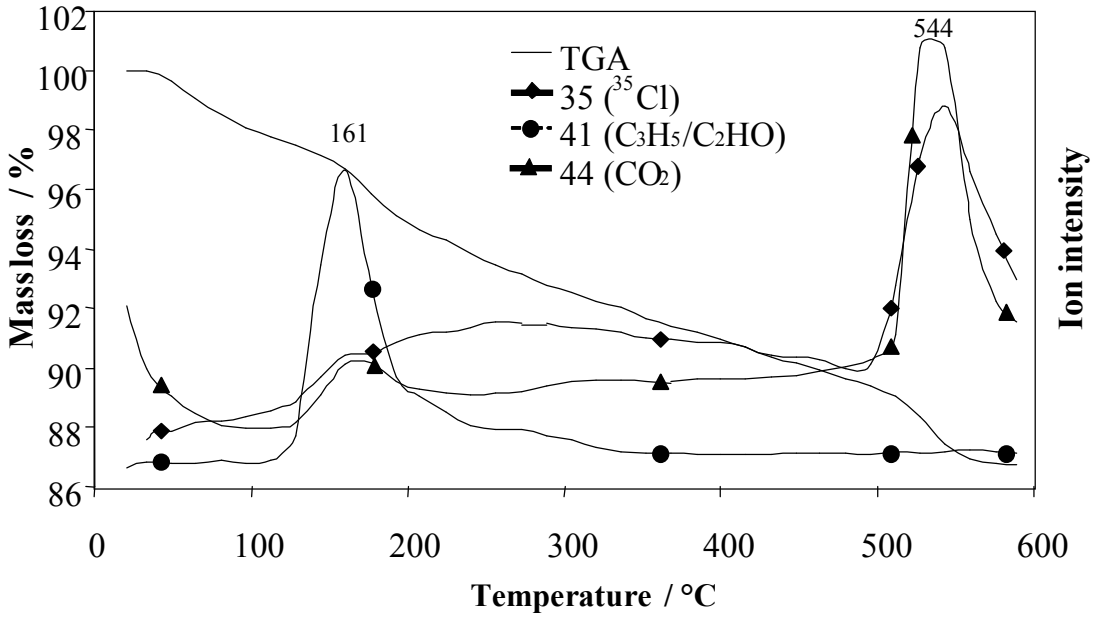

Figure 1. Kristóf *et al.*

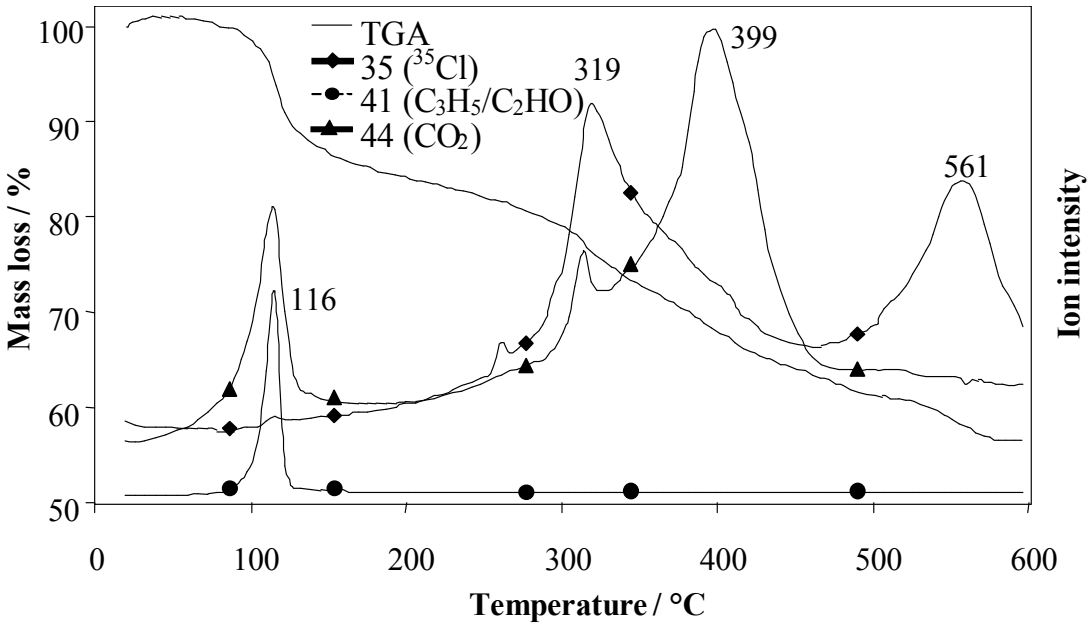

Figure 2. Kristóf *et al.*

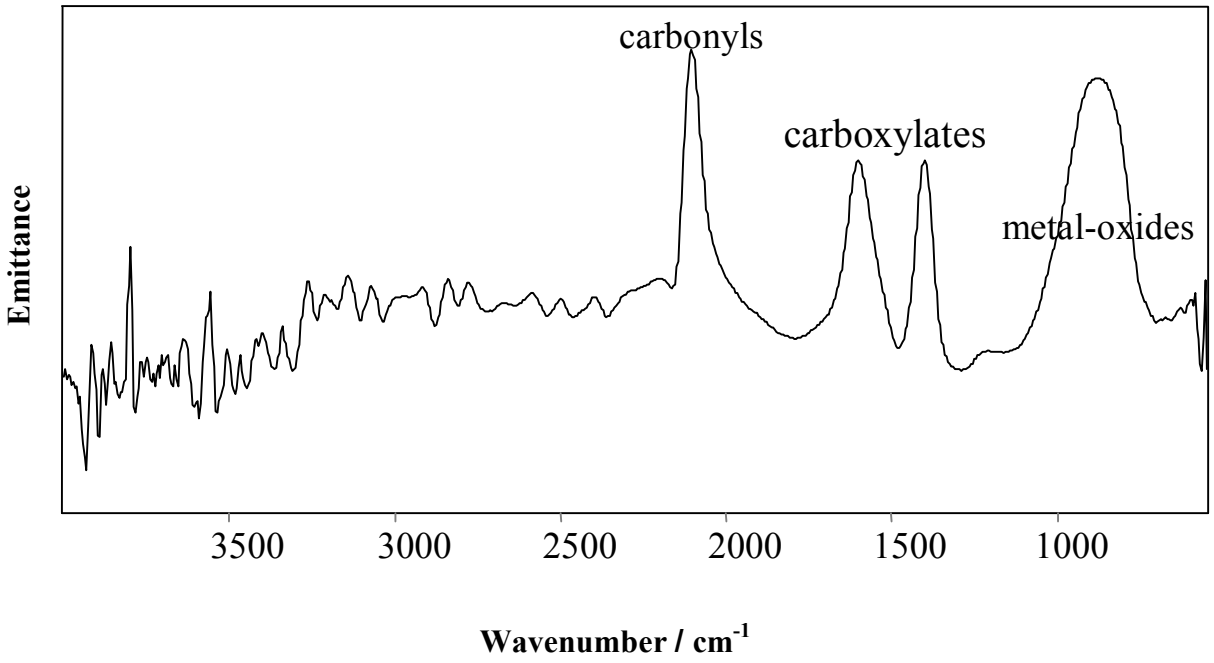

Figure 3. Kristóf *et al.*

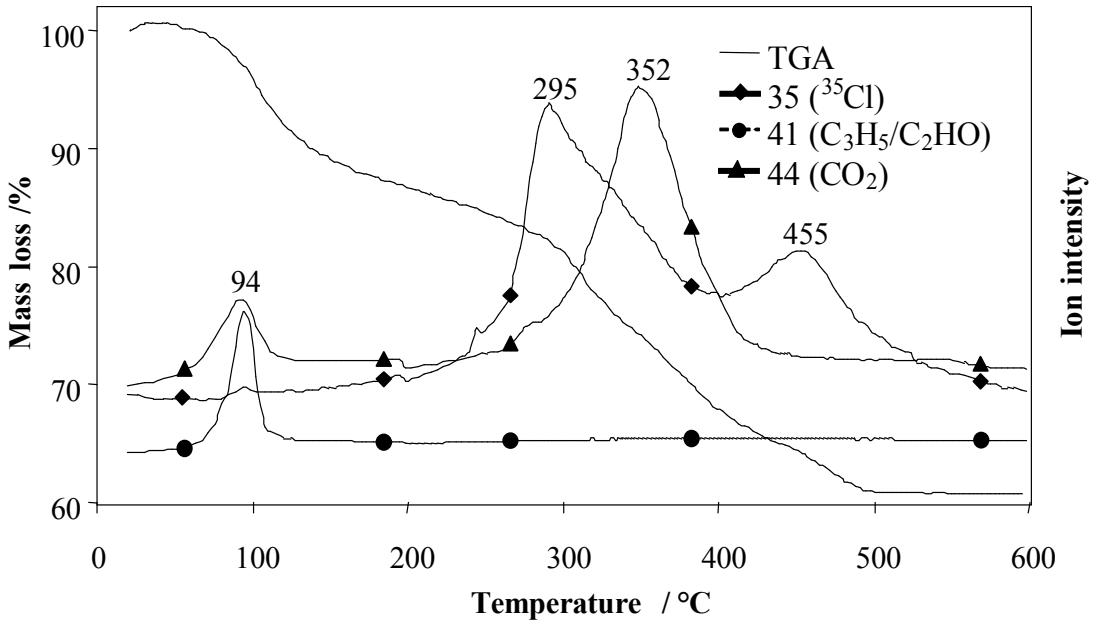

Figure 4. Kristóf *et al.*

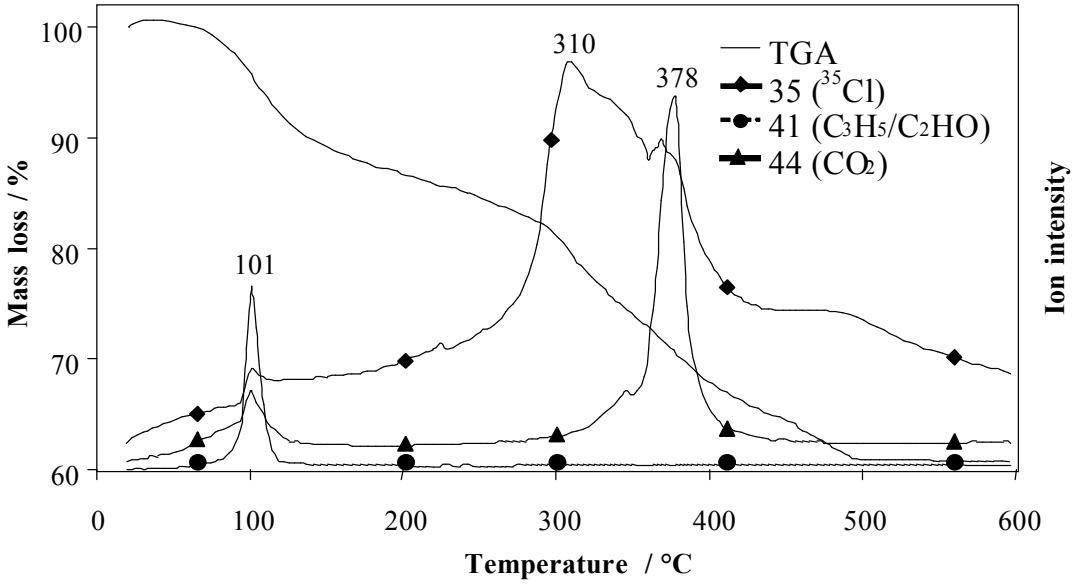

Figure 5. Kristóf *et al.*

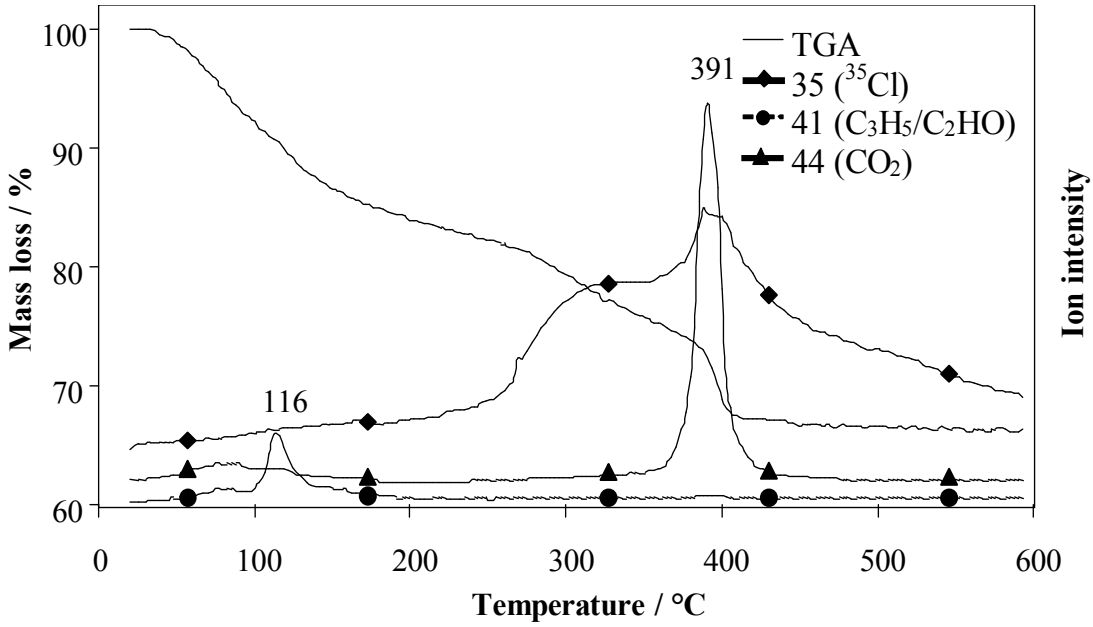

Figure 6. Kristóf *et al.*

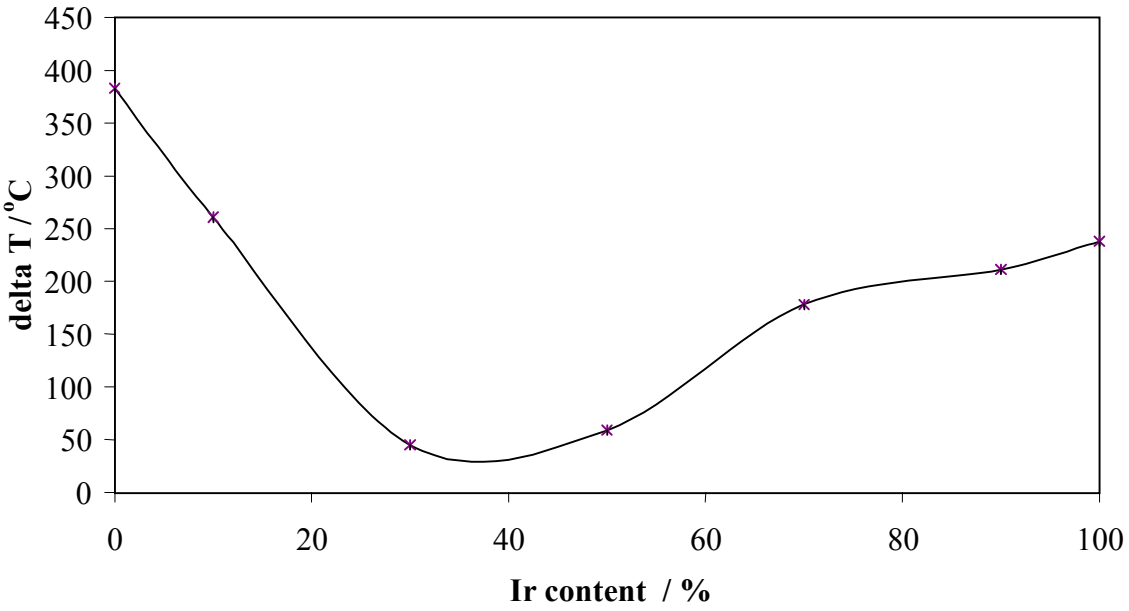

Figure 7. Kristóf *et al.*

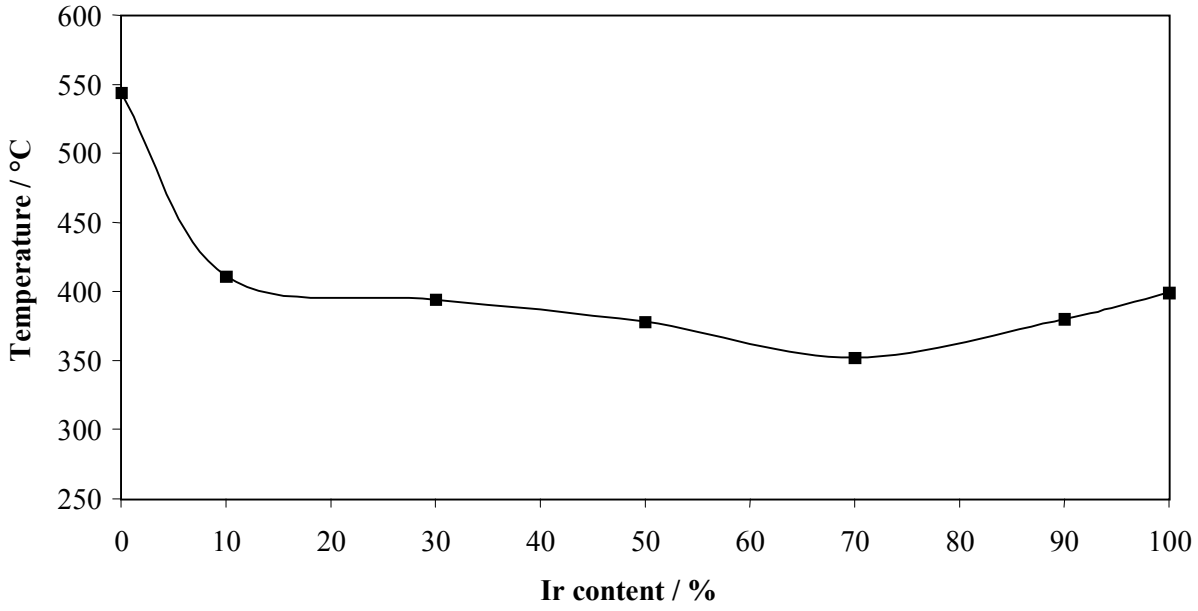

Figure 8. Kristóf *et al.*

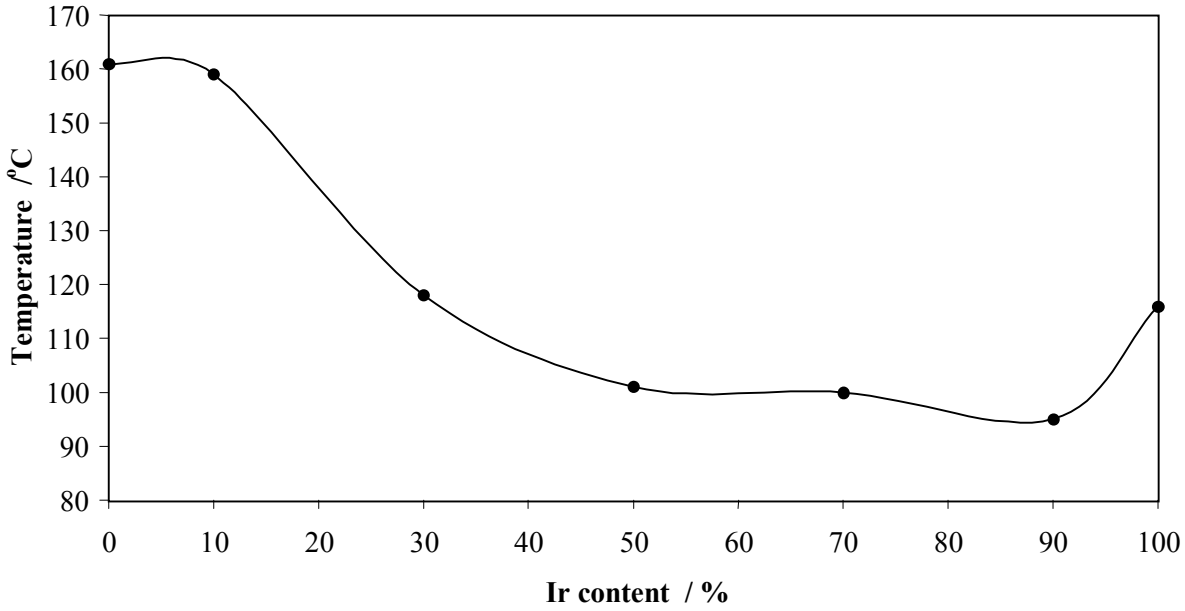

Figure 9. Kristóf *et al.*